View metadata, citation and similar papers at core.ac.uk

brought to you by CORE

provided by St Andrews Research Repository

Accepted Manuscript

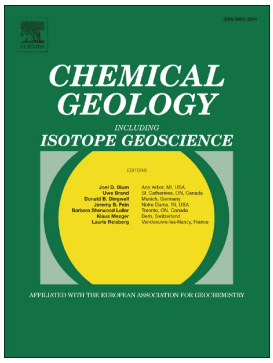

Split-grain 40Ar/39Ar dating: Integrating temporal and geochemical data from crystal cargoes

B.S. Ellis, D.F. Mark, J. Troch, O. Bachmann, M. Guillong, A.J.R. Kent, A. von Quadt

PII: S0009-2541(17)30118-3
DOI: doi: 10.1016/j.chemgeo.2017.03.005
Reference: CHEMGE 18273

To appear in: *Chemical Geology*

Received date: 12 December 2016
Revised date: 6 February 2017
Accepted date: 1 March 2017

Please cite this article as: B.S. Ellis, D.F. Mark, J. Troch, O. Bachmann, M. Guillong, A.J.R. Kent, A. von Quadt , Split-grain 40Ar/39Ar dating: Integrating temporal and geochemical data from crystal cargoes. The address for the corresponding author was captured as affiliation for all authors. Please check if appropriate. Chemge(2017), doi: 10.1016/j.chemgeo.2017.03.005

This is a PDF file of an unedited manuscript that has been accepted for publication. As a service to our customers we are providing this early version of the manuscript. The manuscript will undergo copyediting, typesetting, and review of the resulting proof before it is published in its final form. Please note that during the production process errors may be discovered which could affect the content, and all legal disclaimers that apply to the journal pertain.

ACCEPTED MANUSCRIPT

Split-grain $^{40}Ar/^{39}Ar$ dating: integrating temporal and geochemical data from crystal cargoes

[1]Ellis B.S., [2,3]Mark D.F., [1]Troch J., [1]Bachmann O., [1]Guillong M., [4]Kent A.J.R., [1]von Quadt A.

[1]Institute for Geochemistry and Petrology, ETH Zurich, 8092 Zurich, Switzerland

[2]Isotope Geoscience Unit, Scottish Universities Environmental Research Centre (SUERC), Rankine Avenue, East Kilbride, Scotland, G75 0QF, UK

[3]Department of Earth & Environmental Science, School of Geography & Geosciences, University of St Andrews, St Andrews, KY16 9AJ, UK

[4]College of Earth, Ocean, and Atmospheric Sciences, 104 Ocean Admin., Oregon State University, Corvallis, Oregon, 97330, U.S.A.

Revised version for Chemical Geology

Corresponding author:

Ben Ellis

Institute for Geochemistry and Petrology,

ETH Zurich, 8092 Zurich,

Switzerland

Email: ben.ellis@erdw.ethz.ch

Phone: +41 44 632 99 73

ACCEPTED MANUSCRIPT

ACCEPTED MANUSCRIPT

Abstract

Large sanidine crystals from the Mesa Falls Tuff (MFT), Yellowstone volcanic field, have been split and individually dated via high-precision $^{40}Ar/^{39}Ar$ geochronology with the undated portions further analysed for major elements, trace elements, Pb and Sr isotopes in the sanidine and trace elements in the melt inclusions. This allows the geochemical and geochronological identity of an individual sanidine to be combined. Our MFT sanidines return a preferred eruption age of 1.3011 ± 0.0015/0.0016 Ma (2-sigma, *n*=56, MSWD 0.8, analytical / full external) with a significant component of subtly older (up to ~2 Ma) crystals. Combined with recent results (Rivera et al. 2016, Journal of Petrology 57, 9, 1677-1704) our data define a global mean sanidine $^{40}Ar/^{39}Ar$ age for the MFT of 1.3022 ± 0.0006/0.0008 Ma (2 sigma, analytical / full external) relative to Alder Creek sanidine at 1.1891 Ma and total λ_{40Ar} 5.5305e-10, which gives R_{ACs}^{MFT}: 1.09542 ± 0.00050. The ability to couple geochemistry and geochronology from a single grain allows us, for the first time, to evaluate the origin of the subtly older sanidines present in the same pumices as juvenile sanidines. Melt inclusions from all Mesa Falls sanidines represent extremely fractionated melts with low Sr contents (max. 12 ppm, *n*=39), and rare earth element patterns which require that they be formed from an A-type magma rather than the preceding subduction-related Eocene volcanism as previously suggested. $^{87}Sr/^{86}Sr$ from juvenile and subtly older sanidines shows the same range of 0.7073 to 0.7096, illustrating the susceptibility of such low-Sr melts to slight degrees of assimilation. Pb isotopic compositions are more restricted and identical between the juvenile and subtly older sanidines in the Mesa Falls Tuff ($^{207}Pb/^{206}Pb$ 0.900-0.903, $^{208}Pb/^{206}Pb$ 2.217-2.226, *n*=83) and these compositions rule out the underlying Huckleberry Ridge Tuff member B as a potential source for the subtly older sanidine. LA-ICPMS $^{206}Pb/^{238}U$ dating of Mesa Falls zircons supports no role for the Huckleberry Ridge Tuff. Rather, these subtly older sanidines are interpreted as containing excess mantle-derived Ar. The ability to couple the geochemical and geochronological records within individual sanidine crystals that we demonstrate here has potential to provide new insights for a variety of petrological studies such as diffusional modelling.

ACCEPTED MANUSCRIPT

Keywords: Ar/Ar geochronology, split grain, radiogenic isotopes, Yellowstone, crystal cargo

1. Introduction

With the increasing appreciation that most (if not all) magmatic systems represent open rather than closed systems, the challenge for igneous petrology has become how to best exploit the complex geochemical records found within a single volcanic deposit. Open system behaviour may be observed in a variety of ways, most commonly it is exhibited in the complex crystal cargo evident in many volcanic rocks. Complexity in crystals has been reported in major elements, trace elements, and in-situ isotopic measurements (Davidson et al. 2007; Charlier et al. 2007; Stelten et al. 2015). With the advent of isotopic micro-sampling and so called 'crystal isotope stratigraphy' (e.g. Davidson et al. 2007 and references therein), it appears that with rare exceptions isotopic heterogeneity is pervasive (e.g. Knesel et al. 1999). The ability to geochemically fingerprint individual crystals and zones within crystals allows for different crystal populations to be discriminated. These populations are most typically referred to as phenocrystic (i.e. that grew from the melt in which they are found), antecrystic (precursor grains which grew in an earlier part of the magmatic system) and xenocrystic (foreign grains), yet even such distinctions are complicated as each term comes laden with implied meaning. Thus, the history of a population of grains within a single deposit is challenging to unravel.

Recent improvements in geochronological techniques, particularly in the realm of ID-TIMS U/Pb and $^{40}Ar/^{39}Ar$ geochronology are allowing the timescales of magmatic processes to be investigated in unprecedented detail (e.g., Schmitz and Kuiper, 2013). This improved precision on individual measurements is allowing subtle differences in the ages of individual grains to be recognised and is serving to highlight the role of antecrystic material during petrogenesis. Sluggish diffusion within zircon allows the growth of the crystal, reflecting the magmatic history, to be tracked in both compositional and temporal space with either in-situ measurements (Wotzlaw et al. 2014, 2015) or a combination of in-situ and bulk isotope dilution measurements (e.g. Rivera et al. 2014; Szymanowski et al. 2016). This coupling of compositional information with high-precision geochronology provides a powerful toolkit with which to investigate magmatic processes, yet hitherto it has been most fully utilised with zircon. The generation of the highest precision $^{40}Ar/^{39}Ar$ ages

ACCEPTED MANUSCRIPT

involves the total fusion or step-heating of a potassium-rich mineral phase (typically sanidine/anorthoclase or biotite). However, conventional approaches to dating using $^{40}Ar/^{39}Ar$ methods have required that compositional and chronological information be retrieved from different grains (i.e., data are disconnected). This disconnect can lead to a situation whereby the same crystal could be considered phenocrystic or antecrystic depending on the analytical method employed. The importance of this distinction is of particular importance for diffusion-based studies where zoning patterns in crystals are used to infer timescales of processes immediately pre-eruption (e.g. Morgan and Blake 2006; Till et al. 2015).

This paper for the first time retrieves geochemical and textural information from a population of sanidine grains which are also dated via high precision $^{40}Ar/^{39}Ar$, and compares the chronological record in sanidine to that derived from zircons (via LA-ICPMS) to illuminate how large-volume magmas are generated using the Mesa Falls eruption from Yellowstone as a case study.

2. Geological Background

The Yellowstone volcanic field is the present-day manifestation of a long-lived thermal anomaly in the inland northwest of North America which has produced the Earth's youngest large igneous province. Volcanism began with the Columbia River flood basalts which began erupting ~16.5 Ma from a series of vents in northern Nevada and eastern Oregon (Hooper et al. 2007). Synchronously, rhyolitic volcanism was occurring from widely spread sources across Oregon, Idaho and Nevada (Coble and Mahood 2012). At approximately 14.5 Ma, silicic volcanism became focussed along the track of the Snake River Plain with a broadly time-transgressive evolution of volcanism from south-western Idaho from the Bruneau-Jarbidge eruptive centre and surroundings through the central Snake River Plain to the Heise and Yellowstone eruptive centres. This time-transgressive rhyolitic activity produced numerous large-volume eruptions which are found as ignimbrite sheets on the margins of the plain (e.g. Ellis et al. 2012a; Knott et al. 2016) and as tephra deposits which are found across much of the western U.S.A. (Perkins and Nash 2002; Nash et al. 2006). Presently, the hotspot lies directly under

ACCEPTED MANUSCRIPT

the Yellowstone volcanic field as illustrated by the high heat flow and abundant geothermal activity (see review by Lowenstern et al. 2006).

----INSERT FIGURE 1 location map with chemistry inset----

The Yellowstone volcanic field has evolved episodically over the past ~ 2 Ma with three large-volume eruptions (the Huckleberry Ridge Tuff, Mesa Falls Tuff, and Lava Creek Tuff) separated by periods of relative quiescence during which rhyolitic and basaltic lavas were erupted (Christiansen 2001). The Mesa Falls Tuff (MFT) covers ~2,700 km^2 of south-eastern Idaho and western Wyoming (Fig. 1) with an estimated bulk volume of 280 km^3 (Christiansen 2001). It consists of a series of parallel-bedded fallout deposits of well-sorted, angular, framework-supported pumice and coarse ash beds overlain by a non to weakly-welded ignimbrite containing a variety of lithic clasts. The MFT is a high-silica rhyolite (75.8-77.8 wt.% SiO_2; Fig. 1) with a mineral assemblage containing sanidine + quartz + plagioclase + augite + fayalite + ilmenite + magnetite and accessory zircon and apatite as is typical for Yellowstone rhyolites. Isotopically, the MFT has bulk $^{87}Sr/^{86}Sr_i$ of 0.7084-0.7088 (Doe et al. 1982), εNd of -10.1 (Nash et al. 2006), and $^{206}Pb/^{204}Pb$ of 17.26, $^{207}Pb/^{204}Pb$ of 15.56, and $^{208}Pb/^{204}Pb$ of 38.25 (Doe et al. 1982). In terms of stable isotopes, the MFT is normal in terms of $\delta^{18}O$, as is usual for the larger eruptions at Yellowstone (Bindeman and Valley 2001).

3. Methods

The samples used for this study were collected from a classic locality of the MFT exposed on the west side of highway 20, approximately 6 km north of the town of Ashton, Idaho (Fig. 1). Large single sanidine crystals up to 1 cm in diameter were separated from larger fragments of pumice with crystals hand-picked under a binocular microscope. Crystal surfaces show no evidence of alteration and were typically transparent. Selected sanidines were then cleaned using dilute HNO_3. Grains without adhering glass and the fewest melt inclusions were selected for further work. Sanidines were split into

ACCEPTED MANUSCRIPT

smaller fragments (typically two, but occasionally three or four) using a clean razor blade and a fragment less than 2 mm in diameter was selected for $^{40}Ar/^{39}Ar$ dating with the other fragments placed into separate labelled vials for geochemical analyses (Fig. 2). The grains for $^{40}Ar/^{39}Ar$ dating were then individually re-cleaned in methanol to remove any debris from the cutting process.

----INSERT FIGURE 2 of grains cut----

3.1 $^{40}Ar/^{39}Ar$ geochronology

$^{40}Ar/^{39}Ar$ analyses were conducted at the NERC Argon Isotope Facility, Scottish Universities Environmental Research Centre (SUERC). Details of irradiation durations, irradiation correction factors and discrimination corrections are provided in appendix file SF#1 (.xls).

Two dating experiments were conducted, which required samples to be irradiated in separate batches. Experiment 1: bulk sanidine separates harvested from the MFT ignimbrite (90118) and MFT fallout (90116) were loaded in two large wells in an Al disc for irradiation. Alder Creek sanidine was loaded in to 4 wells surrounding the two samples to allow accurate determination of the J-parameter. These samples were irradiated in the CLICIT facility of the OSU reactor for 120 minutes. These samples were analysed prior to progressing to phase II (split grain approach). Experiment 2: approximately 12 months later the grain fragments produced from cutting the large sanidine crystals (90118) were loaded into a 21 pit Al disc for irradiation (5 discs in total). Each single fragment had its own well position (17 fragments in each Al disc). For J determinations Alder Creek sanidine was loaded into 5 different positions (centre, top, bottom, left, right – see SF#1) in each Al disc. This allowed for determination of an accurate J-parameter for each individual disc. These samples were irradiated in the CLICIT facility of the OSU reactor for 120 minutes.

Single crystals of Alder Creek sanidine (ACs) were fused using a CO_2 laser and the argon isotope composition of cleaned extracted gases analysed using a MAP 215-50 noble gas mass spectrometer using methods described by Mark et al. (2008) and Smith et al. (2011). For determination

ACCEPTED MANUSCRIPT

of the J parameter for each Al disc the weighted average $^{40}Ar^*/^{39}Ar_K$ was calculated for each well, and the arithmetic mean and standard deviation of the $^{40}Ar^*/^{39}Ar_K$ for all standard wells from each different Al disc were used to characterise the neutron fluence for the unknowns. This approach was deemed sufficient, as due to the relatively short irradiation durations there was no significant horizontal variation in J-parameter across the irradiation holder.

The unknown samples were analysed in exactly the same way as the standards. The standard and unknowns were measured within a couple of days of each other. Background and mass discrimination measurements (via automated analysis of multiple air pipettes) specific to each batch are summarised in appendix file SF#1 (.xls). Air pipettes were run (on average) after every 5 analyses. Backgrounds were measured following every two measurements and subtracted from ion beam measurements were arithmetic averages and standard deviations. Mass discrimination was computed based on a power law relationship (Renne et al., 2009) using the isotopic composition of atmospheric Ar (Lee et al., 2006) that has been independently confirmed (Mark et al., 2011). Corrections for radioactive decay of ^{39}Ar and ^{37}Ar were made using the decay constants reported by Stoener et al. (1965) and Renne and Norman (2001), respectively. Ingrowth of ^{36}Ar from decay of ^{36}Cl was corrected using the $^{36}Cl/^{38}Cl$ production ratio and methods of Renne et al. (2008) and was determined to be negligible. Argon isotope data corrected for backgrounds, mass discrimination, and radioactive decay and ingrowth are given in the appendix file SF#1 (.xls).

Ages were computed from the blank-, discrimination- and decay-corrected Ar isotope data after correction for interfering isotopes based on the following production ratios, determined from fluorite and Fe-doped $KAlSiO_4$ glass: $(^{36}Ar/^{37}Ar)Ca = (2.650 \pm 0.022) \times 10^{-4}$; $(^{38}Ar/^{37}Ar)Ca = (1.96 \pm 0.08) \times 10^{-5}$; $(^{39}Ar/^{37}Ar)Ca = (6.95 \pm 0.09) \times 10^{-4}$; $(^{40}Ar/^{39}Ar)K = (7.3 \pm 0.9) \times 10^{-4}$; $(^{38}Ar/^{39}Ar)K = (1.215 \pm 0.003) \times 10^{-2}$; $(^{37}Ar/^{39}Ar)K = (2.24 \pm 0.16) \times 10^{-4}$. Ages and their uncertainties are calculated using the methods of Renne et al. (2010), the decay constant parameters of Renne et al. (2011) and the ACs age of Niespolo et al., 2016 (1.1891 ± 0.0008 Ma), except where noted. For some of the age comparisons made herein, contributions from sources of systematic uncertainty (i.e., uncertainties in $^{40}Ar/^{40}K$ of the standard and ^{40}K decay constants) are neglected and only analytical uncertainties in

ACCEPTED MANUSCRIPT

isotope measurements of samples and standards are included. These uncertainties are referred to herein as "analytical precision". For the purposes of this study analytical uncertainties include contributions from uncertainties in the interference corrections because these interference corrections have variable effects due to the slightly variable chemistry of the samples considered. Where not otherwise distinguished, uncertainties are stated as X ± Y/Z, where Y is the analytical uncertainty as defined above, and Z is the full external precision considering both analytical and systematic sources of uncertainty (e.g., decay constant).

3.2 Geochemistry

The sub-grains for geochemistry were imaged on JEOL JSM-6390 SEM at ETH Zurich (full collection of images in supplementary data) prior to analysis. Major elements were determined via electron microprobe at ETH Zurich using analytical conditions of 15 keV and 15 nA with a beam diameter of 10 μm and counting times were shortened for Na and K to avoid element mobility. Trace elements in sanidines, zircons and melt inclusions were determined via LA-ICPMS using a 193 nm ArF Excimer laser from Resonetics coupled to a Thermo Element XR ICPMS at ETH Zurich (full data in supplementary materials). For trace elements, spot sizes were either 67 microns for sanidines or 30 microns for zircons and melt inclusions. NIST-612 was used as a primary standard and GRD-1 as the secondary standard. Trace element data were reduced following procedures described in Szymanowski et al. (2015) and are considered to be precise to better than 5% of the reported value.

Lead isotope compositions in individual sanidine crystals were measured using laser ablation multicollector inductively-couple plasma mass spectrometry (LA-MC-ICP-MS), using a Photon Machines G2 excimer laser ablation system and NuPlasma MC-ICP-MS at Oregon State University. Analytical techniques followed those given in Kent (2008) using Faraday Cup detectors to measure all required isotopes. Analyses were made using a 85 μm laser spot translated at 5 μm/sec and using a pulse frequency of 7 Hz. Measured ratios were corrected for mass bias based on measurement of NIST-612 glass at similar ablation conditions throughout the analysis session, and an accepted value of $^{208}Pb/^{206}Pb = 2.1694$). Multiple replicate analyses of the NIST-612 and BCR-2G standard glasses

ACCEPTED MANUSCRIPT

(full data in supplementary materials) show that measured $^{208}Pb/^{206}Pb$ and $^{207}Pb/^{206}Pb$ ratios are within 0.1% of the accepted values.

Strontium isotope analyses on grain portions were performed at the Institute of Geochemistry and Petrology, ETH Zurich. Samples were digested with concentrated HF/HNO_3 in Teflon beakers; after evaporation the second dissolution step was followed by 6 N HCL. All solutions were evaporated and the dry residues were converted in 2.5 N HNO_3, followed by Sr separation in ion exchange columns. The chromatography technique used PP columns with Sr- and TRU-spec resin. Strontium isotope ratios were measured on a ThermoFisher multi-collector TritonPlus thermal ionization mass spectrometer (TIMS) using single outgassed Re-filaments. Strontium isotopic analysis was conducted in static mode. The Sr isotope ratios are mass fractionation corrected to $^{88}Sr/^{86}Sr = 8.375209$; the NBS-987 standard measurements returned a $^{87}Sr/^{86}Sr$ ratio of 0.710246 ± 0.0000034 (2 SE; n=14) during the period of analysis. In most cases, Rb and Sr concentrations were determined by ID-method using a highly enriched $^{87}Rb/^{84}Sr$ spike, while in other cases the Rb and Sr contents derived from LA-ICPMS determinations were used. $^{87}Sr/^{86}Sr$ ratios were age-corrected using either the precise age of the individual grain, or in rare cases an assumed age of 1.3 Ma. All results are provided in supplementary material.

3.3 Zircon U/Pb geochronology

Zircons for U-Pb geochronology were separated from pumices of the MFT via classical magnetic and density separation techniques. A subset of zircons were prepared via chemical abrasion following the procedure of Mattinson (2005) and mounted along with untreated zircons from the MFT to assess the effects of chemical abrasion on zircons of this age. Grains were imaged via cathode luminescence (CL) at the ScopeM facility of ETH Zurich using a FEI Quanta 200 FEG scanning electron microscope. Following CL imaging, both chemically abraded and untreated zircons were analysed via LA-ICPMS with the whole procedure of analysis and data reduction following that described by Guillong et al. (2014).

ACCEPTED MANUSCRIPT

4. Results

4.1 $^{40}Ar/^{39}Ar$ sanidine geochronology

The two samples selected for conventional $^{40}Ar/^{39}Ar$ dating, the MFT ignimbrite (#90118) and the MFT fallout (#90116), yield ages of 1.3017 ± 0.0040 Ma and 1.2993 ± 0.0033 Ma, respectively (2-sigma, analytical precision). Both samples showed extensive contamination with crystals older than the defined juvenile population with large numbers of individual data points (ages) rejected from calculation of the weighted mean eruption age, 74% for the ignimbrite and 25% for the fallout. The occurrence of subtly older sanidine crystals has been observed in a number of other studies of Yellowstone rhyolites including deposits erupted both explosively and effusively (Gansecki et al., 1996; Ellis et al., 2012b; Rivera et al., 2014; Stelten et al., 2015; Matthews et al., 2015; Troch et al., 2017). Owing to the large degree of contamination and the data not defining clear juvenile age populations, the Mass Spec programme was used to screen the data to provide an age using the 'youngest gaussian' filter with a MSWD probability cutoff of 0.05.

Owing to the large degree of antecrystic contamination in the ignimbrite we focussed on this sample for the follow-up study – the split grain work (#91235-#91309) to investigate the linking of geochemical-geochronological data for the same grain. Taking this group of split grains as a whole sample population, they define an $^{40}Ar/^{39}Ar$ age of 1.3015 ± 0.0022 Ma (2 sigma, analytical precision). The same statistical filter was used for these data as above. As expected, a large percentage (67%) of the data were rejected from calculation of the mean eruption age for the split grains, attesting to the presence of a significant older population.

Because of the unique way the split grains were irradiated and given the range of sanidine ages, the potential for grain to grain variability in J-value to be affecting the calculated age should be addressed. Even following splitting, the grains within this study remain relatively large (Fig. 2) and so it is conceivable that some grains may be acting to shield others from the fast neutron bombardment during irradiation. We can evaluate the potential for this in two different ways. Firstly, when the

ACCEPTED MANUSCRIPT

calculated ages of grains are plotted against pan position during irradiation (supplementary figure 4), no relationship is apparent. Secondly, the amount of ^{39}Ar can be plotted against age of the grain to test whether shielding of the interior of large grains is occurring. The lack of correlation between the amount of ^{39}Ar and the age of the crystal suggests that this is not an issue.

The ^{40}Ar/^{39}Ar ages for samples from the two experiments are indistinguishable. We have thus determined a global weighted average ^{40}Ar/^{39}Ar age for the MFT: 1.3011 ± 0.0015/0.0016 Ma (2-sigma, *n*=56, MSWD 0.8). This eruption age for the Mesa Falls Tuff is in excellent agreement with the published ID-TIMS zircon ages (Wotzlaw et al. 2015; Rivera et al. 2016) and with the most recent ^{40}Ar/^{39}Ar age of Rivera et al. (2016). We note that the ^{40}Ar/^{39}Ar of Rivera et al. (2016) is calculated using a different Alder Creek sanidine age (Rivera et al. 2013) and a different decay constant (Min et al., 2000). Despite the use of different calibrations the data are indistinguishable. The data of Rivera et al. (2016) recalculated relative to the calibration employed by this study becomes 1.3027 ± 0.0009 Ma (analytical precision), which is indistinguishable (1.6 ± 1.3 ka) from our age for MFT. Taking both datasets (this study and Rivera et al., 2016), we can calculate a global mean age for the MFT of 1.3022 ± 0.0006/0.0008 Ma (2 sigma), which defines R_{ACs}^{MFT}: 1.09542 ± 0.00050.

----INSERT FIGURE 3 new Ar/Ar geochronology----

4.2 Sanidine textural and compositional data

Individual grain sizes for the 'geochemistry sub-grains' were typically in the range of a few hundred microns (images of all grains used for in-situ geochemistry in supplementary materials). Backscattered electron images indicate limited compositional zonation and that about 60% of the crystals contain melt inclusions, which make up less than 5% of the observed section (e.g. grains 2, 5, 42, and 66 in supplementary materials). The frequency of melt inclusions in the geochemistry sub-grains was heightened by them being excluded from the portions of crystals sent for dating.

ACCEPTED MANUSCRIPT

In terms of major element compositions, the Mesa Falls sanidines (*n*=166) show little variation with compositions of Or_{59-63} and no coherent sense of zonation within a crystal. These compositions and the occurrence of major elemental homogeneity within a crystal agree well with previously reported MFT sanidine data (Gansecki et al., 1998). Unlike the major elements, trace elements in the Mesa Falls sanidines do show large compositional ranges which in the most extreme case, Ba, span two orders of magnitude (69-8721 ppm). Large ranges are also observed in Ti (34-104 ppm), Sr (26-209 ppm) and Rb (91-152 ppm). Interestingly, despite the large compositional range between grains, no coherent sense of zonation is observed when plotting rims against cores of individual grains, nor is there compositional variability as a function of crystal age. While our analyses are best efforts at analysing rims and cores of grains, we note with the split grain method the discrimination of rims and core of grains without concentric zonation remains problematic. Nevertheless, given the number of grains (*n*=84) in this study, it is likely that the true compositional range of Mesa Falls sanidine has been characterised.

----INSERT FIGURE 4 Compositional data ----

Melt inclusions hosted in Mesa Falls sanidines are large and homogeneous (as shown in supplementary material) allowing for trace elemental determinations to be carried out via LA-ICPMS. The melt inclusions within the sanidines are similar to other Yellowstone glasses (e.g. Vazquez et al. 2009) and represent extremely fractionated rhyolite liquids as illustrated by the low Sr contents of 2-12 ppm and strong negative Eu anomaly (Fig. 5). Overall, the relatively flat normalised rare earth element (REE) patterns of the MFT melt inclusions are identical to those observed in other rhyolites of the province (e.g. Szymanowski et al. 2015) and in contrast to the steeper patterns observed from subduction zone rhyolites. Notably, REE patterns in glassy melt inclusions are identical between juvenile and subtly older sanidine grains (Fig. 5).

ACCEPTED MANUSCRIPT

----INSERT FIGURE 5 REE in melt inclusions----

4.3 Radiogenic isotopes

Sanidine within the MFT exhibits only slight variability between grains, with $^{208}Pb/^{206}Pb$ ratios spanning 2.217-2.226 and $^{207}Pb/^{206}Pb$ ratios spanning 0.900-0.903 (full data in supplementary materials). The majority of this variability is contained within the precision of the measurements (taken as 2 standard errors) and sanidine LA-ICPMS values are in good agreement with the bulk Pb isotopic data for the Mesa Falls Tuff published by Doe et al. (1982). When compared to all Pb isotopic data from the Yellowstone volcanic field (Fig. 6), it is clear that the Mesa Falls Tuff exhibits relatively little variability. In Pb isotopic space all sanidines appear identical within analytical precision, regardless of the age of the crystal (Fig. 6).

----INSERT FIGURE 6 Pb isotope data for MFT and all Yellowstone----

Mesa Falls sanidines show a large degree of isotopic variability in $^{87}Sr/^{86}Sr$ with 35 grains covering a range from 0.707355 ± 0.000167 to 0.709558 ± 0.000012 (Fig. 7, full data in supplementary material). That the range in $^{87}Sr/^{86}Sr$ is significantly larger than that displayed via Pb isotopes (above) is unsurprising given the relatively low Sr contents of the Yellowstone rhyolitic liquid (2-11 ppm in the melt inclusions), rendering them extremely susceptible to small degrees of contamination. Indeed, such Sr isotopic variability appears relatively common in rhyolites (Charlier et al. 2007; Davidson et al. 2007). The $^{87}Sr/^{86}Sr$ does not appear to be related to the trace elemental identity of the crystal with variations in Ba contents of more than 5,000 ppm observed between crystals with identical isotope ratios. Such decoupling of trace elements from isotopes may be a result of the variable effects of cumulate remelting which readily returns elements sequestered in cumulates (such as Ba and Sr) to the melt without significantly altering isotopic compositions (e.g. Wolff et al. 2015). As might be expected when comparing sub-crystal scale compositions to averages of whole

ACCEPTED MANUSCRIPT

pumice clasts, the range of $^{87}Sr/^{86}Sr$ returned from the split grains is significantly greater than the values of bulk Mesa Falls Tuff of 0.7084 and 0.7088 (Doe et al. 1982) and the 0.70868 of Hildreth et al. (1991).

----INSERT FIGURE 7 Sr variability in here----

4.4 The record from zircon

Zircons from the MFT commonly show oscillatory zonation in CL images with a lack of notably bright zones or dark cores (images in supplementary material). In terms of trace element composition, Ti contents vary from below detection limit (in two cases) to 16 ppm which is similar to the range observed previously for Yellowstone zircons (Rivera et al. 2014, 2016; Stelten et al. 2015; Wotzlaw et al. 2015; compositional data are provided in supplementary materials). While analyses optimised for trace elemental abundances did not return high U and Th values, some spots analysed for U-Pb did find elevated values similar to those observed by Bindeman et al. (2008) in their two Mesa Falls analyses.

LA-ICPMS $^{206}Pb/^{238}U$ ages derived for zircons from the MFT range from 1.133 ± 0.073 Ma to 1.634 ± 0.079 Ma (individual uncertainties at 2 standard error). As illustrated in Figure 8, with the exclusion of three outliers from the total population of 65 grains that were used for final age determination, the average ages of the chemically abraded and untreated grain populations are indistinguishable. However, as is shown in the supplementary material, the proportion of discarded analyses due to common Pb contamination is significantly reduced following chemical abrasion. The distribution of ages is close to a normal distribution. It is therefore possible to report a single crystallisation age of the zircons of 1.322 ± 0.024 Ma. While this age is within uncertainty of the preferred eruption ages defined by both $^{40}Ar/^{39}Ar$ and ID-TIMS (Fig. 3), the higher precision ID-TIMS measurements of Wotzlaw et al. (2015) and Rivera et al. (2016) provide better estimates of eruption age. The value of the LA-ICPMS ages provided here is that the oldest age returned is 1.634 Ma.

ACCEPTED MANUSCRIPT

Zircon ages older than the inferred eruption age have been reported from the SIMS study of Bindeman et al. (2008) that returned zircon core ages of 1.45 ± 0.03 Ma and 1.49 ± 0.05 Ma and a single rim age of 1.49 ± 0.05 Ma. The ID-TIMS studies of Wotzlaw et al. (2015) and Rivera et al. (2016) report zircon ages as old as 1.327 ± 0.017 Ma and 1.568 ± 0.011 Ma respectively.

----Figure 8 Zircon U-Pb diagram----

5. Discussion

5.1 The origin of 'too old' sanidine

Clearly the MFT, in addition to all other Yellowstone rhyolites so far dated via $^{40}Ar/^{39}Ar$ (e.g. Gansecki et al. 1998; Ellis et al. 2012b; Rivera et al. 2014, 2016; Stelten et al. 2015; Matthews et al. 2015; Troch et al. 2017), contains sanidines that are slightly, but distinctly, 'too old' to be considered juvenile to the magma in which they erupted. Below we assess the potential reasons for the presence of this older sanidine.

5.1.1 Entrainment of pre-existing material

One potential source of older sanidines within the Mesa Falls Tuff would be the country rocks through which the Mesa Falls magma transited en-route to the surface. For such material to be incorporated in the MFT magma and not be fully re-equilibrated would require the material to be taken in only a few months prior to eruption. Diffusional calculations for Yellowstone rhyolites by Gansecki et al. (1996) indicate that even xenocrysts of 1000 Ma would return juvenile ages after immersion of only several years in the magma. Gansecki et al. (1996) proposed that the older sanidine and plagioclase they observed was sourced from the Eocene Absaroka volcanics and older basement rocks, on the basis of slightly more anorthitic plagioclase compositions (up to An_{40}) and rare $^{40}Ar/^{39}Ar$ ages as old as 370 Ma but more commonly around 25-50 Ma. The use of the 'split-grain' approach allows us to address this

ACCEPTED MANUSCRIPT

by looking at compositions of melt inclusions within the dated sanidines. It is clear that all of the sanidines in our study crystallised from A-type rhyolitic magmas as illustrated by the relatively flat REE patterns with steep negative Eu anomalies (Fig. 5) and the relatively low Sr contents (e.g. Vazquez et al., 2009), rather than melts generated from subduction-related magmatism. The lack of Eocene ages in our LA-ICPMS U/Pb zircon dataset further suggest limited incorporation of significantly older materials, consistent with other studies of Yellowstone zircon (e.g. Bindeman et al. 2008; Watts et al 2012; Stelten et al. 2015). Gansecki et al. (1996) proposed that the slightly higher anorthite contents of the plagioclase may reflect a subduction-related origin, but such compositions are readily observed within the earlier Yellowstone-related volcanism in the Snake River Plain (Ellis et al. 2013). We speculate that the pre-Yellowstone ages reported by Gansecki may be a consequence of using a 'degassed' basalt to promote coupling between clear feldspar and laser during these early analyses.

Alternatively, the 'too old' sanidine could result from entrainment of slightly older volcanism from the Yellowstone episode. The pre-MFT geology is poorly known, particularly in the area of the caldera which would have been devastated by the MFT eruption. It is entirely conceivable that this region contained numerous rhyolitic lavas and tuffs, which are no longer preserved. The potential for such preservation bias is clear; the pre-MFT record is poorly known at Yellowstone, with only 6 small volume lavas (5 post Huckleberry Ridge Tuff and the earlier Snake River Butte lava) known (Christiansen 2001). When compared to the post Lava Creek Tuff record of volcanism, where at least 40 separate rhyolitic units are known from a roughly equivalent period of time, the difference is stark. Based on the mapped distributions of rhyolites from Yellowstone, a likely potential substrate for entrainment would be Huckleberry Ridge Tuff member B, which underlies the whole source region of the MFT (Christiansen 2001; Fig. 6). The majority of the 'too old' sanidines have ages intermediate between those of the MFT and the HRT which would allow partial re-equilibration of the Ar inventory during the period between entrainment and eruption. Although in many cases (e.g. major elements and trace elements) compositional information derived from the sanidines may be equivocal, the Pb isotopic record demonstrates that there is no contribution from HRT member B (Fig. 6). This conclusion is supported by the U-Pb measurements in zircon (even at the relatively low precision

ACCEPTED MANUSCRIPT

afforded by LA-ICPMS), which preclude significant involvement of HRT with none of the 65 zircons measured here (either in the chemically abraded or untreated populations) returning an age >2 Ma which could have crystallised in the HRT (Fig. 8). However, it is noteworthy that the Island Park lava dome series, which erupted from the same caldera system immediately following the MFT eruption, have Pb isotopic compositions in sanidines which are identical to MFT (Troch et al. 2017) suggesting a localised geographic isotopic signature.

5.1.2 Excess Ar

An alternative explanation for the subtly older sanidine ages in the MFT could be the existence of excess Ar disseminated either within fluid inclusions or within defects in the crystal lattice (e.g. Esser et al. 1997; Renne et al. 1997; Winick et al. 2001; Stelten et al. 2015). The lack of observable fluid inclusions within sanidines during inspection under a binocular microscopes suggests the excess Ar component may reside within the crystals themselves. The excess Ar explanation is attractive because it allows for juvenile and 'too old' sanidines within the MFT to have the identical geochemistry and Pb isotopic compositions, with only the age being disturbed, as illustrated in Figure 9. Studies of the gas and fluid geochemistry of the Yellowstone system have commonly detected a mantle component, principally in $^{3}He/^{4}He$ (e.g. Craig et al. 1978) with recent work also documenting the role of thermal metamorphism of cratonic lithologies in contributing to the degassing budget (Lowenstern et al. 2014). Taking a mantle $^{40}Ar/^{36}Ar$ value of 40,000 (Burnard et al. 1997; Graham 2002; illustrated in Fig. 9), the involvement of excess, mantle-derived Ar within the MFT sanidines could readily explain the 'too-old' sanidine. While partial re-equilibration of sanidine sourced from the Huckleberry Ridge Tuff could also produce a data array similar to that observed in Fig. 9, however the Pb isotopic compositions of the sanidines within the MFT (see above) preclude recycling from HRT member B. If the subtly older sanidines in the MFT are indeed due to the presence of excess Ar, this feature highlights the difficulty in using the term 'antecryst'. We note that previous studies dating MFT sanidine using step-heating (Lanphere et al. 2002; Rivera et al. 2016) found older ages in the lower temperature steps that in the case of the Lanphere et al. (2002) study were interpreted as excess Ar.

ACCEPTED MANUSCRIPT

While these older ages could be interpreted as re-entrainment of older components of the same magmatic system the total overlap in all geochemical and isotopic parameters measured here would require the recycled material to be compositionally identical to the juvenile component. The ability to directly couple the age of the sanidine to the compositional information contained in the crystal and discriminate between these two possibilities (i.e. antecrystic vs. excess Ar) highlights the utility of the new split grain method.

----INSERT FIGURE 9 Inv. Isochron----

5.2 Generation of the Mesa Falls Tuff

The combination of geochemical, isotopic, and geochronological records from sanidine and zircon allows the petrogenesis of the MFT to be investigated in greater detail. The steep negative Eu anomaly and low Sr contents in MFT melt inclusions indicate that both the Eu and Sr have been sequestered into plagioclase during earlier stages of evolution and subsequently removed by fractionation. In terms of radiogenic isotopes, bulk Sr, Nd, and Pb isotopic values (Doe et al. 1982; Hildreth et al. 1991), Nd isotopes in glass separates (Nash et al. 2006), Hf isotopes in zircons (Wotzlaw et al. 2015), and the Pb and Sr analyses from sanidines all indicate limited contributions from surrounding crustal lithologies, particularly given the strong isotopic leverage provided by the Archean Wyoming craton (Doe et al. 1982). Indeed, the requirement of crustal contamination to pass from typical Yellowstone basalt to MFT-like compositions is slight. The large variability observed within sanidines in $^{87}Sr/^{86}Sr$ space is typical of the isotopic heterogeneity observed in many large silicic magmatic systems (e.g. Charlier et al. 2007) and results from the rhyolitic liquids with low Sr contents being particularly susceptible to assimilation. Published oxygen isotopes reveal a normal-$\delta^{18}O$ magma (Hildreth et al. 1984; Bindeman and Valley 2001) in contrast to much of the younger volcanism at Yellowstone. The normal- $\delta^{18}O$ signature along with the trace elemental and radiogenic isotopic evidence above indicates that the

ACCEPTED MANUSCRIPT

MFT, like the other large-volume explosive rhyolites at Yellowstone, may most simply be explained as a magma generated by fractional crystallisation-dominated processes with limited assimilation.

5.3 Potential of the split-grain method

The MFT data raise interesting questions for crystal-specific studies as the similarity in appearance, major and trace elemental composition of the subtly older crystals within the MFT makes their distinction without the associated high-precision geochronology impossible. The requirement to define the provenance of crystals is also clear for analytically challenging projects involving radiogenic isotopes or diffusional modelling whereby necessarily few crystals are typically studied (e.g. Knesel et al. 1999; Morgan et al. 2006; Till et al. 2015). We note that in the studies referred to, the target mineral was sanidine and we propose that the split-grain method outlined here has the potential to generate exciting avenues of research coupling geochronology and geochemistry in major phases.

6. Conclusions

The main conclusions of this study are:

1. For the first time, we demonstrate that it is possible to couple high-precision $^{40}Ar/^{39}Ar$ geochronology with in-situ major, trace and isotopic determinations of sanidines using the split-grain approach. This technique has significant potential to help understand the complex age spectra often observed in volcanic rocks. Indeed, the geochemical aspect of the split-grain approach could readily be extended to include other avenues of research such as diffusion modelling in sanidine, O isotopic studies, or determination of volatile contents of melt inclusions as appropriate to the sample.

2. By combining geochemical, isotopic, and chronological information from sanidines, for the first time we illustrate how by interpreting the data separately (i.e. just the $^{40}Ar/^{39}Ar$ data or just the trace element or isotopic data) may affect the interpretation of the same population of crystals.

ACCEPTED MANUSCRIPT

3. The $^{40}Ar/^{39}Ar$ data indicate the 'too old' sanidine grains contain excess Ar, a feature consistent with the elevated $^{3}He/^{4}He$ found in the Yellowstone system. The occurrence of excess Ar explains the compositional and isotopic similarity between juvenile and 'too old' sanidine. Isotopic compositions of the 'too old' sanidine crystals reveals that they do not represent partially re-equilibrated material scavenged from the underlying Huckleberry Ridge Tuff member B. Such a conclusion is only possible using the split grain method described here.

4. Radiogenic and stable isotopic compositions of both bulk samples and individual juvenile sanidines do not require high degrees of any potential assimilant, a conclusion in good agreement with previous studies of the MFT.

Acknowledgements

This work benefitted significantly from discussions with John Wolff, the comments of an anonymous reviewer and editorial handling from Don Dingwell. We thank the ETH Zurich ScopeM microscopy centre for assistance with CL imaging. NERC is acknowledged for continued funding of AIF at SUERC, East Kilbride. This work was supported by an ETH research grant (ETH-05 13-2) and funds from Swiss National Science Foundation research grants (SNSF 200021-146268 and SNSF 200021-155923/1) and US National Science Grant 1425491.

References

Bindeman, I.N., Valley, J.W., 2001. Low $\delta^{18}O$ rhyolites from Yellowstone: magmatic evolution based on analyses of zircons and individual phenocrysts. J. Petrol. 42, 1491-1517.

Bindeman, I.N., Fu, B., Kita, N., Valley, J.W., 2008. Origin and evolution of Yellowstone silicic magmatism based on ion microprobe analysis of isotopically-zoned zircons. J. Petrol. 49, 163-193.

Burnard, P., Graham, D., Turner G., 1997. Vesicle-Specific Noble Gas Analyses of "Popping Rock": Implications for Primordial Noble Gases in Earth. Science 276, 568-571

ACCEPTED MANUSCRIPT

Charlier, B.L.A., Bachman, O., Davidson, J.P., Dungan, M.A., Morgan, D.J., 2007. The Upper Crustal Evolution of a Large Silicic Magma Body: Evidence from Crystal-scale Rb-Sr Isotopic Heterogeneities in the Fish Canyon Magmatic System, Colorado. J. Petrol. 48, 1875-1894.

Christiansen, R.L., 2001. The Quaternary and Pliocene Yellowstone Plateau volcanic field of Wyoming, Idaho, and Montana. U.S. Geol. Surv. Professional Paper 729-G.

Coble, M.A., Mahood, G.A., 2012. Initial impingement of the Yellowstone plume located by widespread silicic volcanism contemporaneous with Columbia River flood basalts. Geology 40, 655-658.

Craig, H., Lupton J.E., Welham, J.A., Poreda R., 1978. Helium isotope ratios in Yellowstone and Lassen Park volcanic gases. Geophys. Res. Lett. 5, 11, 897-900.

Davidson, J.P., Morgan, D.J., Charlier, B.L.A., Harlou, R., Hora, J.M., 2007. Microsampling and isotopic analysis of igneous rocks: implications for the study of magmatic systems. Ann. Rev. Earth and Plan. Sci. 35, 273-311.

Doe, B. R., Leeman, W. P., Christiansen, R. L., Hedge, C. E., 1982. Lead and strontium isotopes and related trace elements as genetic tracers in the upper Cenozoic rhyolite-basalt association of the Yellowstone Plateau volcanic field. J. Geophys. Res. 87, 4785-4806.

Ellis, B.S., Branney, M.J., Barry, T.L., Barfod, D., Bindeman. I., Wolff, J.A., Bonnichsen, B., 2012a. Geochemical correlation of three large-volume ignimbrites from the Yellowstone hotspot track, Idaho, USA. Bull. Volcanol. 74 :261-277.

Ellis, B.S., Mark, D.F., Pritchard, C.J., Wolff, J.A., 2012b. Temporal dissection of the Huckleberry Ridge Tuff using the $^{40}Ar/^{39}Ar$ dating technique. Qua. Geochron. 9, 34-41.

Ellis, B.S., Wolff, J.A., Boroughs, S., Mark, D.F., Starkel, W.A., Bonnichsen, B., 2013. Rhyolitic volcanism of the central Snake River Plain: a review. Bull. Volcanol. 75, 745.

Esser, R.P., McIntosh, W.C., Heizler, M.T., Kyle, P.R., 1997. Excess argon in melt inclusions in zero-age anorthoclase feldspar from Mt. Erebus, Antarctica, as revealed by the $^{40}Ar/^{39}Ar$ method. Geochim Cosmochim Acta. 61, 3789-3801.

Feeley, T.C., Cosca, M.A., Lindsay, C.R., 2002. Petrogenesis and Implications of Calc-Alkaline Cryptic Hybrid Magmas from Washburn Volcano, Absaroka Volcanic Province, USA. J. Petrol., 43, 663-703.

ACCEPTED MANUSCRIPT

Gansecki, C., Mahood, G., McWilliams, M., 1996. $^{40}Ar/^{39}Ar$ geochronology of rhyolites erupted following collapse of the Yellowstone caldera, Yellowstone plateau volcanic field: implications for crustal contamination. Earth Planet. Sci. Lett. 142, 91-107.

Gansecki, C., Mahood, G., McWilliams, M., 1998. New ages for the climactic eruptions at Yellowstone: Single-crystal $^{40}Ar/^{39}Ar$ dating identifies contamination. Geology 26, 343–346.

Graham, D.W., 2002. Noble Gas Isotope Geochemistry of Mid-Ocean Ridge and Ocean Island Basalts: Characterization of Mantle Source Reservoirs. Rev. Mineral. Geochem. 47, 247-319.

Guillong, M., von Quadt, A., Sakata, S., Peytcheva, I., Bachmann, O., 2014. LA-ICP-MS Pb–U dating of young zircons from the Kos–Nisyros volcanic centre, SE Aegean arc. J. Anal. Atom. Spec. 29, 963-970.

Hildreth, W., Christiansen, R. L., O'Neil, J. R., 1984. Oxygen isotopic study of the Yellowstone Plateau volcanic field. J. Geophys. Res. 89, 8339-8369.

Hildreth, W., Halliday, A.N., Christiansen, R.L., 1991. Isotopic and chemical evidence concerning the genesis and contamination of basaltic and rhyolitic magma beneath the Yellowstone Plateau volcanic field. J. Petrol. 32, 63–138.

Hooper, P.R., Camp, V.E., Reidel, S.P., Ross, M.E., 2007. The origin of the Columbia River Flood Basalt province: plume versus non-plume models. In: Foulger, G., and Jurdy (eds.), Plates, plumes and planetary processes. Geol. Soc. Am. Spec. Pap. 430, 635-668.

Kent, A.J.R., 2008. In-situ analysis of Pb isotope ratios using laser ablation MC-ICP-MS: Controls on precision and accuracy and comparison between Faraday cup and ion counting systems. J. Anal. At. Spectrom. 23, 968-975.

Knesel, K.M., Davidson, J.P., and Duffield, W.A., 1999. Evolution of silicic magma through assimilation and subsequent recharge: evidence from Sr isotopes in sanidine phenocrysts, Taylor Creek Rhyolite, NM. J. Petrol. 40, 773-786.

Knott, T.R., Branney, M.J., Reichow, M.K., Finn, D.R., Coe, R.S., Storey, M., Barfod, D., McCurry M., 2016. Mid-Miocene record of large-scale Snake River–type explosive volcanism and associated subsidence on the Yellowstone hotspot track: The Cassia Formation of Idaho, USA. Geol. Soc. Am. Bull. 128, 1121-1146.

ACCEPTED MANUSCRIPT

Lanphere, M.A., Champion, D.E., Christiansen, R.L., Izett, G.A., Obradovich, J.D., 2002. Revised ages for tuffs of the Yellowstone Plateau volcanic field: Assignment of the Huckleberry Ridge Tuff to a new geomagnetic polarity event. Geol. Soc. Am. Bull. 114, 5, 559-568.

Lee, J.Y., Marti, K., Severinghaus, J.P., Kawamura, K., Yoo, H.S., Lee, J.B., Kim, J.S., 2006. A redetermination of the isotopic abundances of atmospheric Ar. Geochim. Cosmochim. Acta 70, 4507-4512.

Lowenstern, J.B., Evans, W.C., Bergfield, D., Hunt, A.G., 2014. Prodigious degassing of a billion years of accumulated radiogenic helium at Yellowstone. Nature 506, 355-358.

Lowenstern, J.B., Smith, R.B., Hill, D.P., 2006. Monitoring super-volcanoes: geophysical and geochemical signals at Yellowstone and other large caldera systems. Phil. Trans. Royal Soc. A364, 2055-2072.

Mark, D.F., Kelley, S.P., Lee, M.R., Parnell, J., Sherlock, S.C., Brown, D.J., 2008. Ar–Ar dating of authigenic K-feldspar: Quantitative modelling of radiogenic argon-loss through subgrain boundary networks. Geochim. Cosmochim. Acta 72(11), 2695–2710.

Mark, D.F., Stuart, F.M., de Podesta, M., 2011. New high-precision measurements of the isotopic composition of atmospheric argon. Geochim. Cosmochim. Acta 75, 7494-7501.

Matthews, N.E., Vazquez, J.A., Calvert, A.T., 2015. Age of the Lava Creek supereruption and magma chamber assembly at Yellowstone based on $^{40}Ar/^{39}Ar$ and U-Pb dating of sanidine and zircon crystals. Geochem. Geophys. Geosyst. 16, doi:10.1002/2015GC005881.

Mattinson, J.M., 2005. Zircon U-Pb chemical abrasion ("CA-TIMS") method: Combined annealing and multi-step partial dissolution analysis for improved precision and accuracy of zircon ages. Chem. Geol. 200, 47-66.

Min, K., Mundil, R., Renne, P.R., Ludwig, K.R., 2000. A test for systematic errors in 40Ar/39Ar geochronology through comparison with U/Pb analysis of a 1.1 Ga rhyolite. Geochem. Cosmochim. Acta, 64, 73-98

Morgan, D.J., Blake, S., 2006. Magmatic residence times of zoned phenocrysts: Introduction and application of the binary element diffusion modelling (BEDM) technique. Contrib. Mineral. Petrol. 151, 58–70, doi: 10.1007/s00410-005-0045-4.

ACCEPTED MANUSCRIPT

Morgan, D.J., Blake, S., Rogers, N.W., De Vivo, B., Rolandi, G., Davidson, J.P., 2006. Magma chamber recharge at Vesuvius in the century prior to the eruption of A.D. 79. Geology 34, 845-848.

Nash, B.P., Perkins, M.E., Christensen, J.N., Lee, D.-C., Halliday, A.N., 2006. The Yellow-stone hotspot in space and time: Nd and Hf isotopes in silicic magmas. Earth Planet. Sci. Lett. 247, 143–156.

Niespolo, E.M., Rutte, D., Deino, A.L., Renne, P.R., 2016. Intercalibration and age of the Alder Creek sanidine $^{40}Ar/^{39}Ar$ standard. Qua. Geochron. *in press* (*online first*).

Perkins, M.E., Nash, B.P., 2002. Explosive silicic volcanism of the Yellowstone hotspot: the ash fall tuff record. Geol Soc Am Bull. 114:367–381

Renne P.R., Deino, A.L., Hames, W., Heizler, M.T., Hemming, S.R., Hodges, K.V., Koppers, A.A.P., Mark, D.F., Morgan, L.E., Phillips, D., Singer, B.S., Turrin, B.D., Villa, I.M., Villeneuve M., Wijbrans J.R., 2009. Data reporting norms for $^{40}Ar/^{39}Ar$ geochronology. Qua. Geochron. 5, 346-352.

Renne, P.R., Norman, E.B., 2001. Determination of the half-life of ^{37}Ar by mass spectrometry. Phys. Rev. C, 63 047302

Renne P.R., Sharp, W.D., Deino A.L., Orsi, G., Civetta, L., 1997. $^{40}Ar/^{39}Ar$ Dating into the Historical Realm: Calibration Against Pliny the Younger. Science 277, 1279-1280

Renne P.R., Sharp, Z.D., Heizler, M.T., 2008. Cl-derived argon isotope production in the CLICIT facility of OSTR reactor and the effects of the Cl-correction in $^{40}Ar/^{39}Ar$ geochronology. Chem. Geol. 255, 463-466.

Renne, P. R., Mundil, R., Balco, G., Min, K., Ludwig, K. R., 2010. Joint determination of ^{40}K decay constants and $^{40}Ar^*/^{40}K$ for the Fish Canyon sanidine standard, and improved accuracy for $^{40}Ar/^{39}Ar$ geochronology. Geochim. Cosmochim. Acta 74, 5349–5367.

Renne P.R., Balco G., Ludwig, K.R., Mundil, R., Min, K., 2011. Response to the comment by W.H. Schwarz et al. on "Joint determination of ^{40}K decay constants and $^{40}Ar^*/^{40}K$ for the Fish Canyon sanidine standard, and improved accuracy for $^{40}Ar/^{39}Ar$ geochronology" by P.R. Renne et al., 2010. Geochim.Cosmochim. Acta 75, 5097-5100.

Rivera, T.A., Schmitz, M.D., Crowley, J.L., Storey, M., 2014. Rapid magma evolution constrained by zircon petrochronology and $^{40}Ar/^{39}Ar$ sanidine ages for the Huckleberry Ridge Tuff, Yellowstone, USA. Geology 42, 643-646.

ACCEPTED MANUSCRIPT

Rivera, T.A., Schmitz, M.D., Jicha, B.R., Crowley, J.L., 2016. Zircon petrochronology and $^{40}Ar/^{39}$ sanidine dates for the Mesa Falls Tuff : crystal-scale records of magmatic evolution and the short lifespan of a large Yellowstone magma chamber. J. Petrol. 57, 9, 1677-1704.

Rivera, T.A., Storey, M., Schmitz, M.D., Crowley, J.L., 2013. Age intercalibration of 40Ar/39Ar sanidine and chemically distinct U/Pb zircon populations from the Alder Creek Rhyolite Quaternary geochronology standard. Chem. Geol. 345, 87-98.

Schmitz, M.D., Kuiper, K.F., 2013. High precision geochronology. Elements 9, 25-30.

Singer, B.S., Jicha, B.R., Condon, D.J., Macho, A.S., Hoffman, K.A., Dierkhising, J., Brown, M.C., Feinberg, J.M., Kidane, T., 2014. Precise ages of the Réunion event and Huckleberry Ridge excursion: Episodic clustering of geomagnetic instabilities and the dynamics of flow within the outer core. Earth Plan. Sci. Lett. 405, 25-38.

Smith, V.C., Mark, D.F., Staff, R.A., Blockley, S.P.E., Ramsey, C., Bryant, C.L., Nakagawa, T., Han, K.K., Weh, A., Takemura, K., Danahara, T., 2011. Toward establishing precise $^{40}Ar/^{39}Ar$ chronologies for Late Pleistocene palaeoclimate archives: an example from the Lake Suigetsu (Japan) sedimentary record. Qua. Sci. Rev. 30, 2845-2850.

Stelten M.E., Cooper, K.M., Vazquez, J.A., Calvert A.T., Glessner J.J.G., 2015. Mechanisms and timescales of generating eruptible rhyolitic magmas at Yellowstone caldera from zircon and sanidine geochronology and geochemistry. J. Petrol. 56, 1607-1642

Stelten M.E., Cooper K.M. Vazquez J.A., Reid, M.R., Barfod G.H., Wimpenney, J., Yin, Q., 2013. Magma mixing and the generation of isotopically juvenile silicic magma at Yellowstone caldera inferred from coupling $^{238}U–^{230}Th$ ages with trace elements and Hf and O isotopes in zircon and Pb isotopes in sanidine. Contrib. Mineral. Petrol. 166, 587-613.

Stoener R.W., Schaeffer, S., Katcoff, S., 1965. Half-lives of argon-37, argon-39, and argon-42. Science 148, 1325-1328.

Szymanowski, D., Ellis, B.S., Bachmann O., Guillong M., Phillips W.M., 2015. Bridging basalts and rhyolites in the Yellowstone – Snake River Plain volcanic province: the elusive intermediate step. Earth Planet. Sci. Lett. 415, 80-89.

ACCEPTED MANUSCRIPT

Szymanowski, D., Ellis, B.S., Wotzlaw, J-F., Buret, Y., von Quadt, A., Peytcheva, I., Bindeman, I.N., Bachmann O., 2016. Geochronological and isotopic records of crustal storage and assimilation in the Wolverine Creek–Conant Creek system, Heise eruptive centre, Snake River Plain. Contrib. Mineral. Petrol. 171 :106.

Till C.B., Vazquez J.A., Boyce J.W., 2015. Months between rejuvenation and volcanic eruption at Yellowstone caldera, Wyoming. Geology 43, 695-698.

Troch J., Ellis, B.S., Mark, D.F., Bindeman, I.N., Kent, A.J., Guillong, M., Bachmann, O., 2017. Rhyolite generation prior to a Yellowstone supereruption: Insights from the Island Park-Mount Jackson rhyolite series. J. Petrol. doi.org/10.1093/petrology/egw071

Vazquez J.A., Kyriazis, S., Reid M.R., Sehler R.C., Ramos, F.C., 2009. Thermochemical evolution of young rhyolites at Yellowstone: Evidence for a cooling but periodically replenished postcaldera magma reservoir. J. Volcanol. Geotherm. Res. 188, 186-196.

Watts, K.E., Bindeman, I.N., and Schmitt, A., 2012. Crystal scale anatomy of a dying supervolcano: An isotope and geochronology study of individual phenocrysts from voluminous rhyolites of the Yellowstone caldera. Contrib. Mineral. Petrol. 164, 45–67, doi:10.1007/s00410-012-0724-x.

Winick, J.A., McIntosh, W.C., Dunbar, N.W., 2001. Melt inclusion-hosted excess ^{40}Ar in quartz crystals of the Bishop and Bandelier magma systems. Geology 29, 275-278.

Wolff J.A., Ellis B.S., Ramos F.C., Starkel W.A., Boroughs S., Olin P.H., Bachmann O., (2015) Remelting of cumulates as a process for producing chemical zoning in silicic tuffs: a comparison of cool, wet and hot, dry felsic magma systems. Lithos 236-237, 275-286.

Wotzlaw, J-F., Bindeman I.N., Stern, R.A., D'Abzac F-X., Schaltegger U., 2015. Rapid heterogeneous assembly of multiple magma reservoirs prior to Yellowstone supereruptions. Sci. Rep. 5, 14026; doi: 10.1038/srep14026.

Wotzlaw, J-F., Bindeman, I.N., Watts, K.E., Schmitt, A.K., Caricchi, L., Schaltegger, U., 2014 Linking rapid magma reservoir assembly and eruption trigger mechanisms at evolved Yellowstone-type supervolcanoes. Geology 42, 807-810.

ACCEPTED MANUSCRIPT

Figures

Figure 1: Location map showing the outcrop of the Mesa Falls Tuff ignimbrite and the inferred source for the deposit (after Christiansen 2001). Inset shows the bulk compositions of the Mesa Falls pumice compared to other Yellowstone rhyolites.

Figure 2: Example of a sanidine grain used in this study (grain 64) illustrating the results of splitting the grains (further examples are in supplementary materials). Schematic beneath illustrates what the various portions of the grains are used for.

Figure 3: $^{40}Ar/^{39}Ar$ ages for the Mesa Falls Tuff with grains in black reflecting those used to estimate the eruptive age of the deposit while those in grey are excluded.

Figure 4: Trace elemental compositions of the sanidines used in the split grain experiment. Vectors on the diagram are those expected from fractional crystallisation and recharge / cumulate melting. As noted in the text, scatter away from the main trend may reflect the difficulty in assigning 'rim' and 'core' compositions to portions of a split grain.

Figure 5: Rare earth element patterns from sanidine-hosted melt inclusions illustrating similar compositions between the antecrystic and phenocrystic grains. Similarity in REE patterns in inclusions indicates that the antecrystic sanidines grew from liquids generated in a similar manner to the juvenile sanidines. Insets show typical normalised REE patterns from the Yellowstone-Snake River Plain province (Ellis et al. 2013) and from the Eocene Washburn volcanic centre (Feeley et al. 2002).

Figure 6: Pb isotope compositions of dated sanidines from the MFT. Notably, the Pb isotopic composition of MFT sanidines does not overlap with the composition of sanidines in Huckleberry Ridge Tuff member B (based on data from Watts et al. 2012 and Stelten et al. 2013). This lack of isotopic agreement comes despite HRT member B outcropping above the inferred source of the MFT, the Henrys Fork caldera (H) illustrated in lower inset map (after Christiansen 2001). Upper inset shows all sanidine Pb isotopic data from Yellowstone.

ACCEPTED MANUSCRIPT

Figure 7: Sr isotopic composition of sanidine from the MFT. Grey bar highlights the bulk $^{87}Sr/^{86}Sr$ values published for MFT by Doe et al. (1982) and Hildreth et al. (1991). The range in $^{87}Sr/^{86}Sr$ is much larger than the range in Pb isotopes (Fig. 6).

Figure 8: U-Pb ages of zircons from the MFT. No zircon dated from the MFT returns an age consistent with crystallisation in the underlying HRT, in agreement with the Pb isotopic results.

Figure 9: Inverse isochron diagram showing the MFT data. The 'too old' sanidines are found in a wedge reflecting the presence of excess Ar, with a mantle $^{40}Ar/^{36}Ar$ of 40,000 (Graham, 2002) illustrated. An inverse isochron based on the age of the Huckleberry Ridge Tuff is shown in purple.

ACCEPTED MANUSCRIPT

ACCEPTED MANUSCRIPT

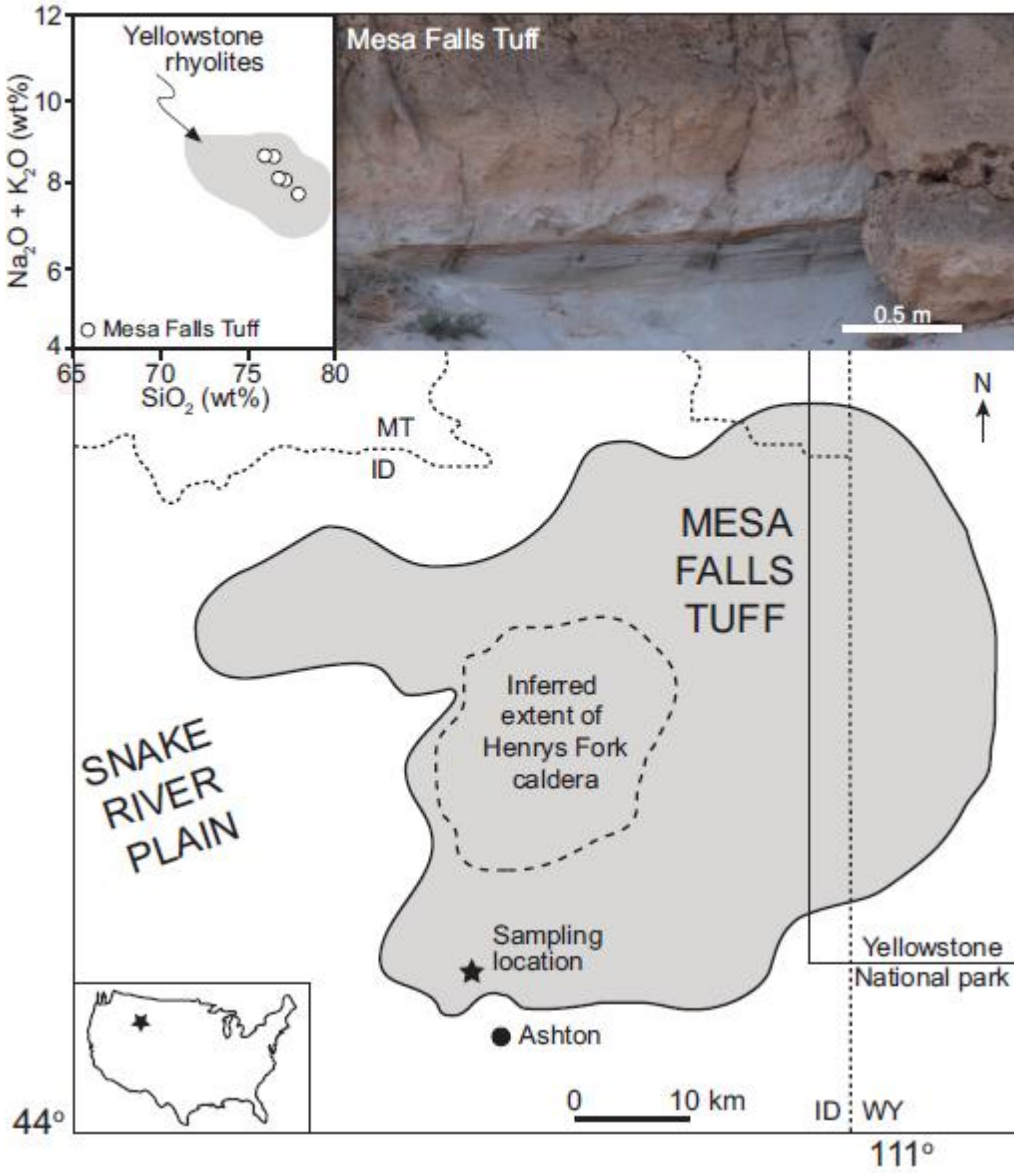

Figure 1

ACCEPTED MANUSCRIPT

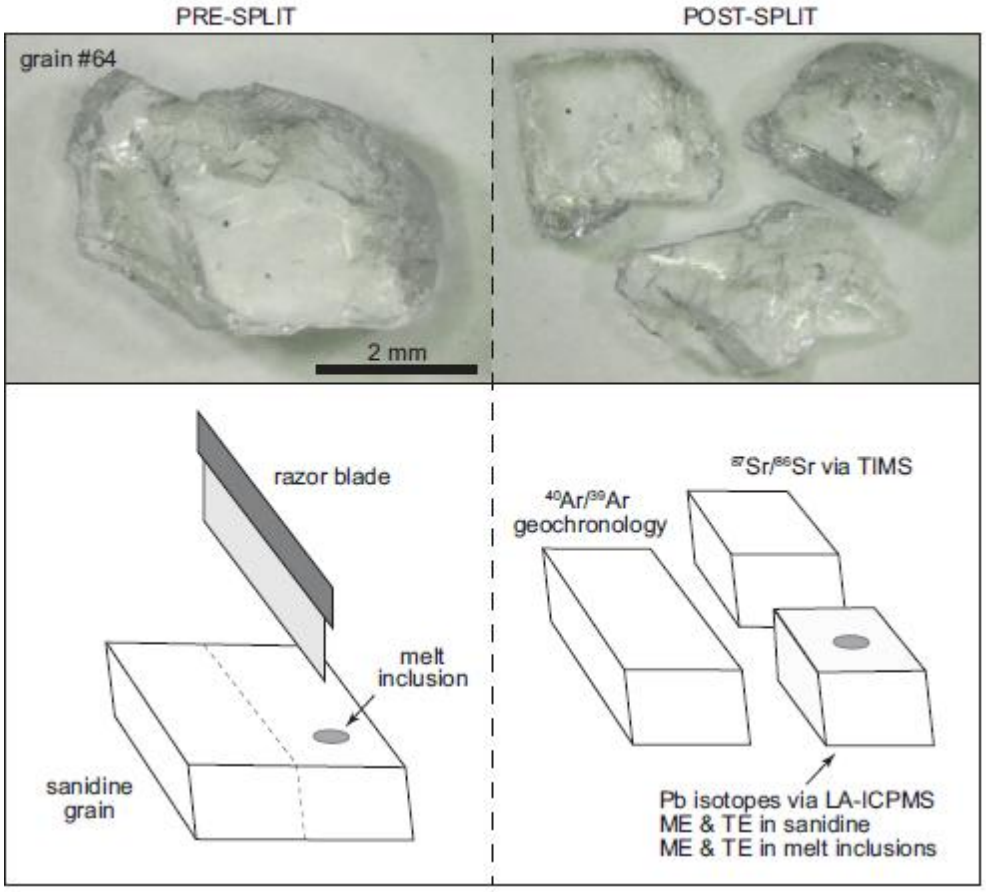

Figure 2

ACCEPT

ACCEPTED MANUSCRIPT

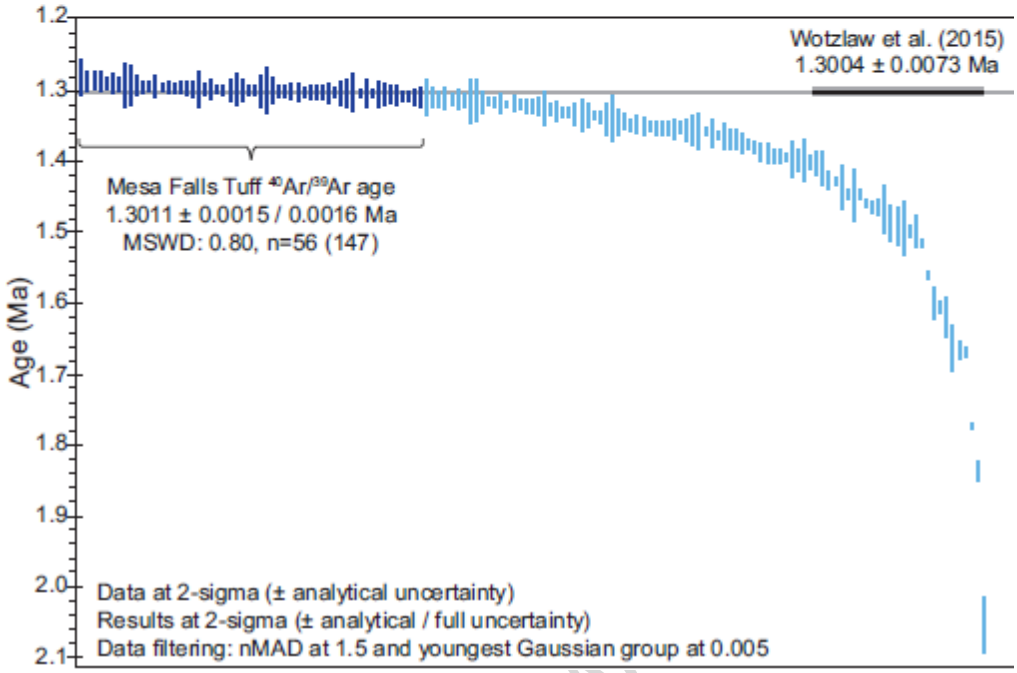

Figure 3

ACCEPTED MANUSCRIPT

ACCEPTED MANUSCRIPT

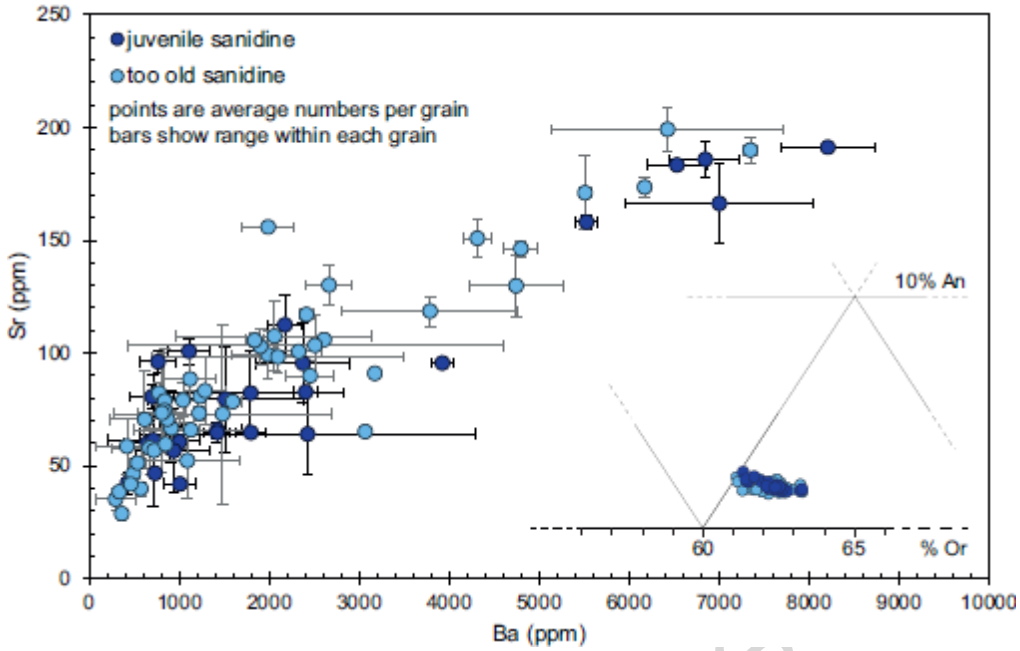

Figure 4

ACCEPTED MANUSCRIPT

ACCEPTED MANUSCRIPT

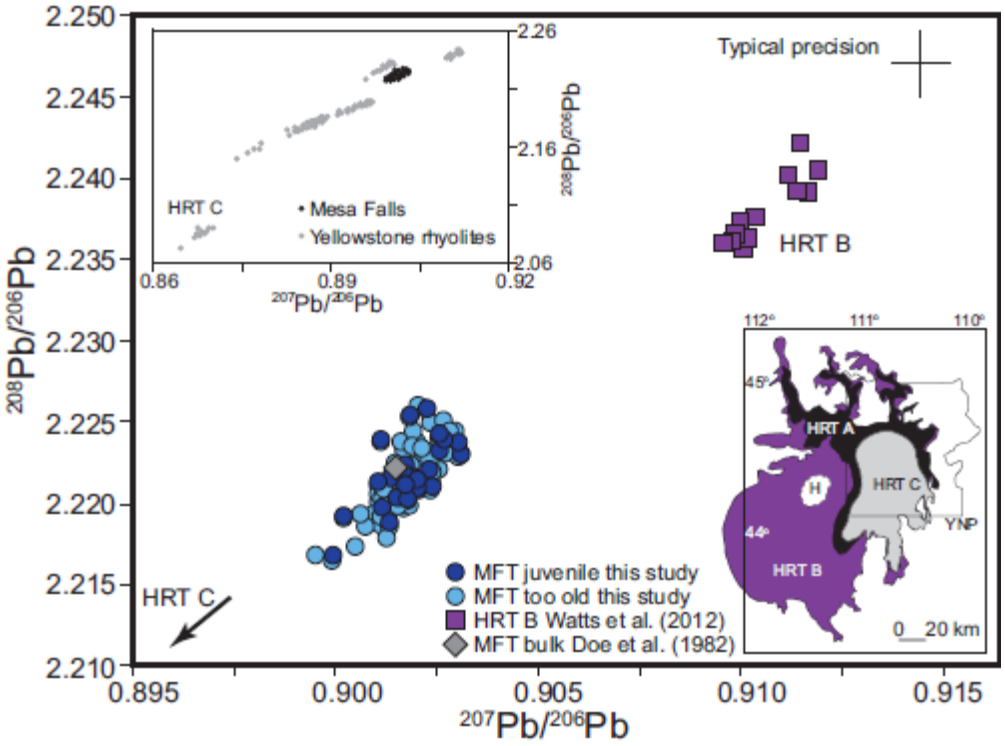

Figure 5

ACCEPTED MANUSCRIPT

ACCEPTED MANUSCRIPT

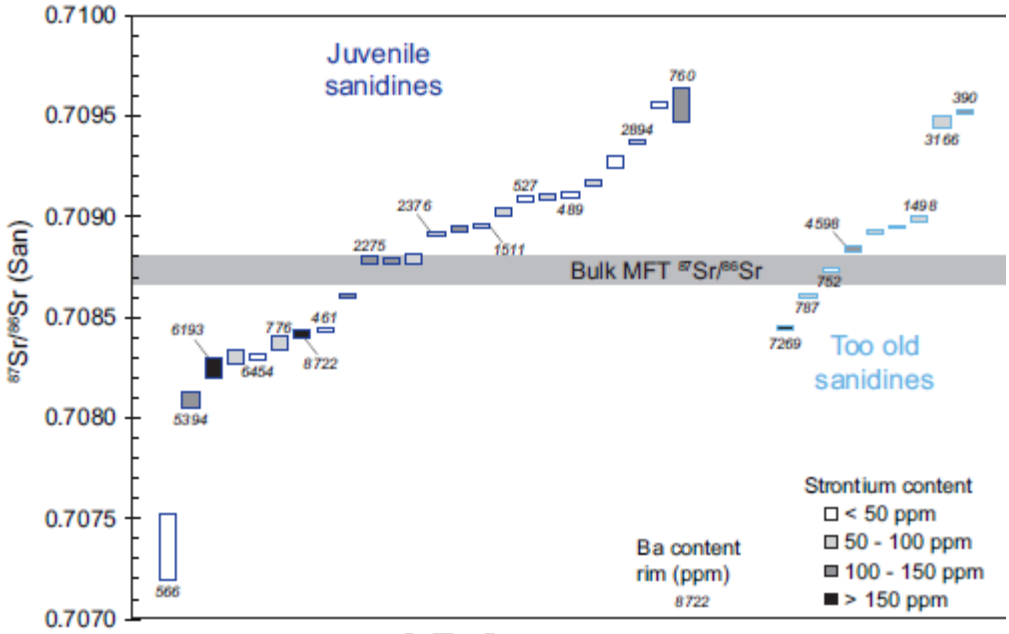

Figure 6

ACCEPTED

ACCEPTED MANUSCRIPT

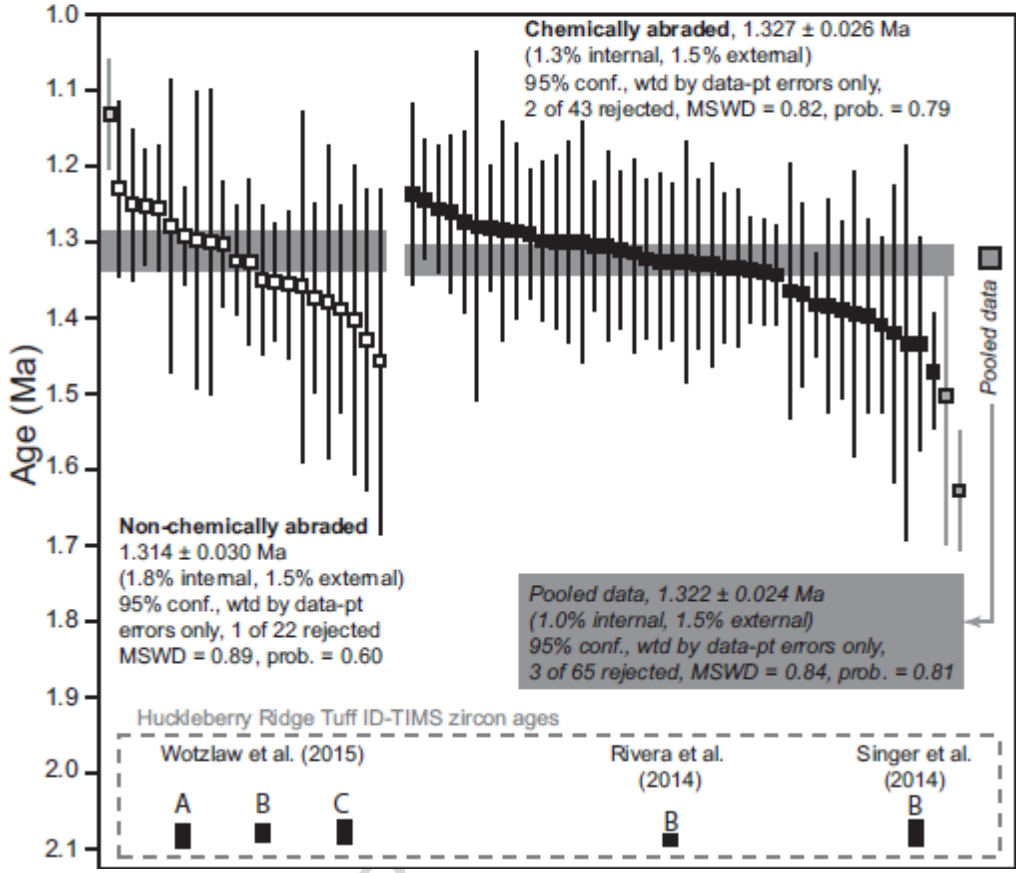

Figure 7

ACCEP

ACCEPTED MANUSCRIPT

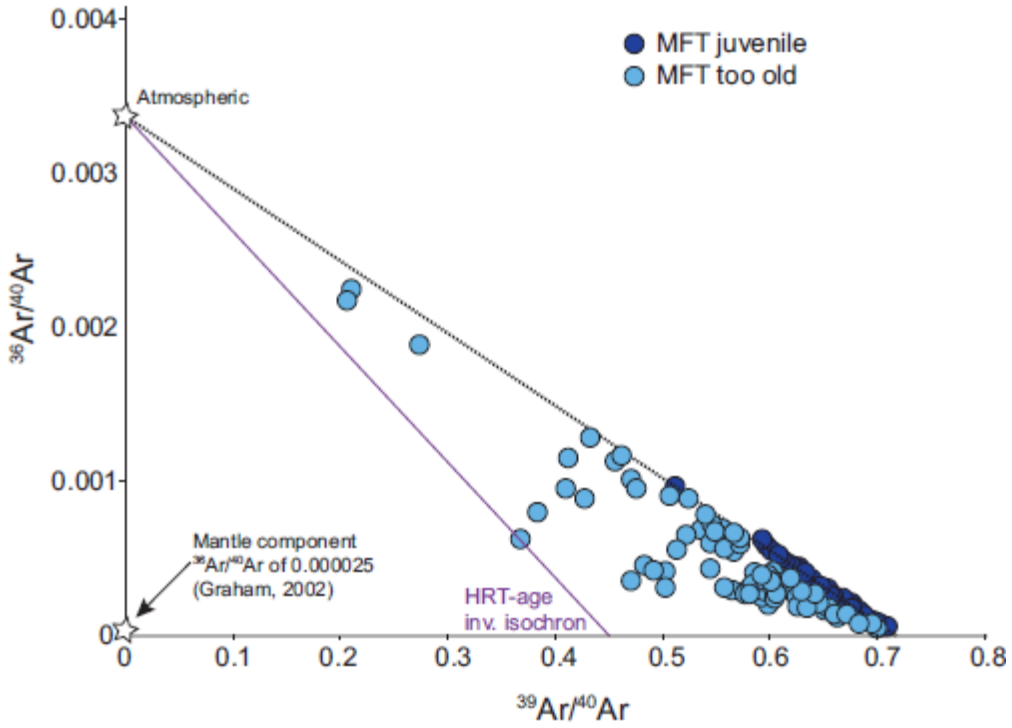

Figure 8

ACCE

ACCEPTED MANUSCRIPT

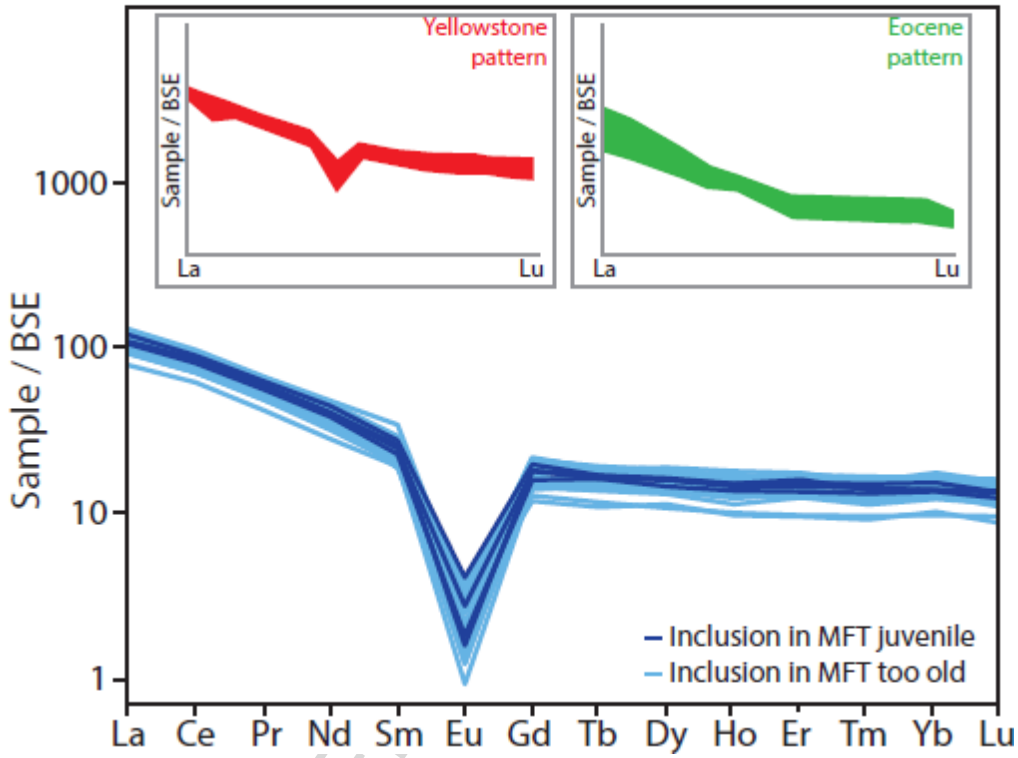

Figure 9

ACCE